NANO LETTERS
Cite This: Nano Lett. XXXX, XXX, XXX−XXX
Letter
pubs.acs.org/NanoLett

An Electrically Actuated, Carbon-Nanotube-Based Biomimetic Ion Pump

Jake Rabinowitz,[†] Charishma Cohen,[†] and Kenneth L. Shepard*[,†,‡]

[†]Department of Electrical Engineering, Columbia University, New York, New York 10027, United States
[‡]Department of Biomedical Engineering, Columbia University, New York, New York 10027, United States

Supporting Information

ABSTRACT: Single-walled carbon nanotubes (SWCNTs) are well-established transporters of electronic current, electrolyte, and ions. In this work, we demonstrate an electrically actuated biomimetic ion pump by combining these electronic and nanofluidic transport capabilities within an individual SWCNT device. Ion pumping is driven by a solid-state electronic input, as Coulomb drag coupling transduces electrical energy from solid-state charge along the SWCNT shell to electrolyte inside the SWCNT core. Short-circuit ionic currents, measured without an electrolyte potential difference, exceed 1 nA and scale larger with increasing ion concentrations through 1 M, demonstrating applicability under physiological (∼140 mM) and saltwater (∼600 mM) conditions. The interlayer coupling allows ionic currents to be tuned with the source−drain potential difference and electronic currents to be tuned with the electrolyte potential difference. This combined electronic−nanofluidic SWCNT device presents intriguing applications as a biomimetic ion pump or component of an artificial membrane.

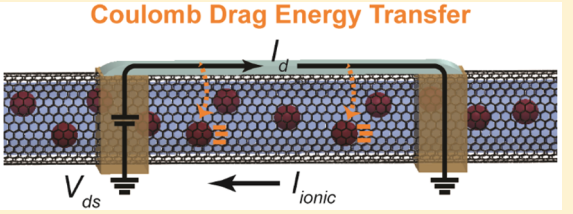

KEYWORDS: *Single-walled carbon nanotubes, Coulomb drag, nanofluidics, synthetic ion pumps, biomimetic ion channels*

Single-walled carbon nanotubes (SWCNTs) are well-established platforms for transporting electronic charge and electrolyte. They can be used as semiconducting channels in electronic field-effect transistors,[1,2] where SWCNT shells have been shown to ballistically transport charge,[3,4] or as electrolyte channels in ionic field-effect transistors,[5] where SWCNT cores efficiently transport fluid.[5−9] In electronic circuits, SWCNTs show tunable conductivity through a back-gate potential, based on modulation of Schottky barriers at metal−SWCNT junctions.[10,11] In ionic circuits, SWCNTs show tunable conductivity through the same gate potential, based on modulation of electrolyte charge within the core.[5] Despite their promise, these electronic and ionic transport capabilities have yet to be integrated into a single SWCNT. Such a device could afford new opportunities in biomimetic ion pumping[12] or artificial membrane engineering.[13]

SWCNTs already have shown promise as synthetic ion channels, where they resemble biological counterparts.[7,9,14] The atomically small SWCNT core rejects macromolecules, and chemical functionalization of SWCNT ends yields selectivity for small counterions.[7,9,15,16] In these prior works, potential differences or pressure gradients drive electrolyte and ions with anomalously large flows, enhanced mobility, and single-file transport.[5,7,9,14−17] In our work, integrating ionic and electronic transistors into individual SWCNTs allows us to transport electrolyte using a solid-state electronic input. This electronic input pumps ions through Coulomb drag energy transfer from electronic currents traversing the shell to electrolyte within the core.

Coulomb drag is an effect where mobile charge across a conductor induces a short-circuit current or open-circuit voltage across a nearby yet electrically isolated conductor.[18−23] Mobile charge in the "drive layer" transfers energy to quiescent charge in the "drag layer", inducing a drag layer current that flows without a supporting potential difference. Coulomb drag has been theoretically[24,25] and experimentally[26,27] demonstrated in SWCNTs by exposing them to fluid flow and measuring corresponding open-circuit voltages. Potential differences across SWCNTs can likewise drive fluid flow, due to the mutual nature of Coulomb interactions.[27] We engineer these Coulomb drag effects to pump ions through SWCNTs without requiring electrolyte potential differences or pressure gradients.

Figure 1a shows the simultaneous employment of a single SWCNT as an ionic and an electronic field-effect transistor. The SWCNT connects two electrolyte reservoirs containing Ag/AgCl pseudoreference electrodes for applying electrolyte potential differences (V_{ionic}) and measuring ionic currents (I_{ionic}). Metal electrodes contact the SWCNT for applying source−drain potential differences (V_{ds}) and measuring electronic currents (I_d). During operation, the source terminal is maintained at equipotential with the electrolyte reservoir on the same side of the SWCNT; V_{ds} and V_{ionic} are applied with respect to these equipotential electrodes, through the drain terminal and opposing electrolyte reservoir (Figure 1b). Interlayer Coulomb coupling arises due to the proximity of

Received: November 4, 2019
Revised: December 9, 2019
Published: December 26, 2019

DOI: 10.1021/acs.nanolett.9b04552
Nano Lett. XXXX, XXX, XXX−XXX

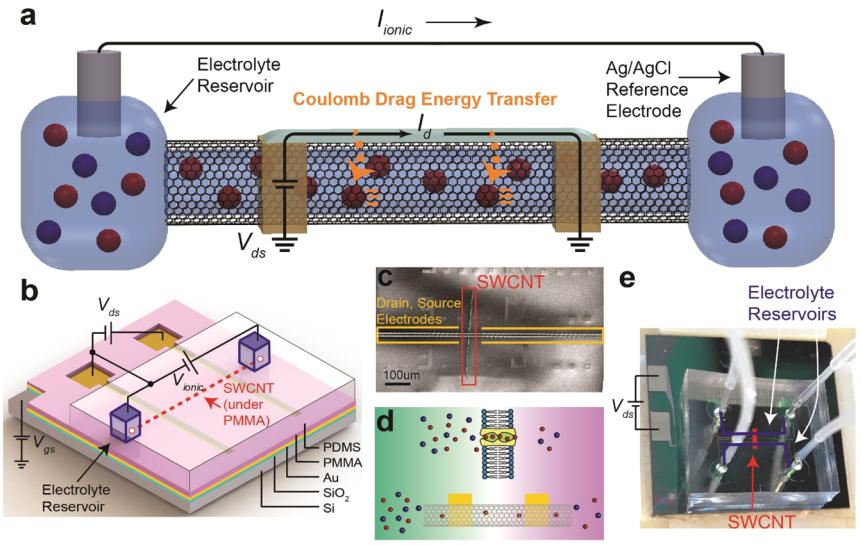

Figure 1. Experimental overview. (a) A single SWCNT connects two electrically isolated circuits. Electronic current (I_d) flows along the SWCNT shell and through gold electrodes, while ionic current (I_{ionic}) flows through the SWCNT core and Ag/AgCl reference electrodes. The proximity of the circuits results in Coulomb drag energy transfer between layers (orange arrows), driving I_{ionic} to flow without an electrolyte potential difference. Currents primarily contain positive charge (holes, cations), such that Coulomb drag coupling is repulsive. (b) Device schematic, illustrating the SWCNT location and application of source−drain (V_{ds}), electrolyte (V_{ionic}), and back-gate (V_{gs}) potential differences. (c) Scanning electron micrograph image of isolated SWCNT with source and drain electrodes. (d) SWCNT exhibiting ion selectivity comparable to biological ion channels, excluding anions and macromolecules. (e) Photograph of a fabricated device. Note: 100 nm gold electrodes appear gray due to thickness.

the ionic and electronic circuits, such that I_{ionic} signals are tunable with V_{ds} and I_d signals are tunable with V_{ionic}.

Because our device leverages Coulomb drag coupling between ionic and electronic currents, it operates as an electrically actuated, biomimetic ion pump. When applying V_{ds}, I_d carriers traversing the SWCNT shell transfer energy to ions within the SWCNT core through Coulomb drag. In turn, ions are pumped without a V_{ionic} potential difference (Figure 1a, orange arrows). The observed Coulomb coupling is consistent with reciprocal energy transfer, showing a similar performance when employing I_d or I_{ionic} as the drive layer signal. Coulomb drag interactions are repulsive due to I_d being hole-dominated and I_{ionic} being cation-dominated.[7,9,16,28,29] In addition to Coulomb drag, interlayer coupling exists through field-effect gating of I_{ionic} with V_{ds} and of I_d with V_{ionic}.

Figure 1b depicts a chip-level schematic of the device (side view in Figure S1). Initially, chemical vapor deposition SWCNTs nucleate and grow from iron catalyst particles over highly doped silicon with thermal oxide. Raman spectroscopy confirms that growth conditions are tuned to yield single-walled carbon nanotubes (Figure S2). After growth, an isolated nanotube is located with scanning electron microscopy and confirmed to be single-walled with atomic force microscopy (Figure S3). Average diameters are 1 nm (Table S1), and lengths are hundreds of μm. Metal electrodes are deposited over suitable SWCNTs (Figure 1c), followed by PMMA patterning to form electrolyte reservoirs and expose SWCNTs to oxygen plasma. Plasma treatment truncates SWCNTs at electrolyte reservoir edges, shortening SWCNTs to tens of μm and functionalizing the outer rings with carboxylic acid groups. These outer rings become negatively charged in solution, yielding selective transport of small cations similar to biological ion channels (Figure 1d). A PDMS cover interfaces the electrolyte reservoirs with external tubing. Electrical contact to the silicon substrate allows for modulation of SWCNT conductivity through the back-gate (V_{gs}) configuration, though V_{gs} is only applied during device verification. A fully fabricated device photograph is provided in Figure 1e.

Control tests verify leakage-free ionic and electronic circuit pathways. Before introducing electrolyte, we verify the electronic circuit by sweeping V_{gs} from −10 to 10 V with V_{ds} = 0.1 V. SWCNTs demonstrate unipolar (p-type) or ambipolar conductivity (Figure S4), findings consistent with intrinsically p-type SWCNTs and electric-field gating of the Schottky barriers at the metal−nanotube contacts.[11,28] Schottky barrier variation across devices is such that I_d ranges from several nA to several uA. Next, we verify the ionic circuit based on observing linear ionic conductance (G_{ionic}) that scales semi-logarithmically with electrolyte concentration (c) as $G_{ionic} \approx c^b$. We extract b from linear fits to log−log conductance−concentration data (Figure S5), where G_{ionic} is calculated from linear I_{ionic}−V_{ionic} measurements (Figure S6, red). Prior SWCNT studies measure $b \approx 1/3$,[5,6] and our experimental values range from 0.22 to 0.37 (Table S1). These measurements confirm that ionic transport through the SWCNT core is observed, rather than through possible leakage paths.

The coupling between the ionic and electronic circuits becomes evident during ion circuit verification. Linear ionic conductance measured with floating metal electrodes (electronic amplifier off) becomes nonlinear when setting V_{ds} = 0 (Figure S6, blue). The rectified I_{ionic} signal is attributed to mismatched Schottky barriers at metal−SWCNT contacts, which are highly sensitive to fabrication conditions.[29] Due to this barrier height mismatch, applying V_{ds} induces asymmetric charge distribution along the SWCNT shell, rectifying I_{ionic}−V_{ionic} and I_d−V_{ds} curves.[30] I_{ionic} magnitudes increase when V_{ds} = 0 (Figure S6), demonstrating that the charge redistribution lowers the energy barrier to ion transport.

To study Coulomb drag ion pumping and interlayer coupling, electrolyte reservoirs are flushed with KCl solutions and V_{ionic} and V_{ds} are swept from −0.3 to 0.3 V in 0.1 V increments (with V_{gs} = 0). At every condition, currents are

DOI: 10.1021/acs.nanolett.9b04552
Nano Lett. XXXX, XXX, XXX−XXX

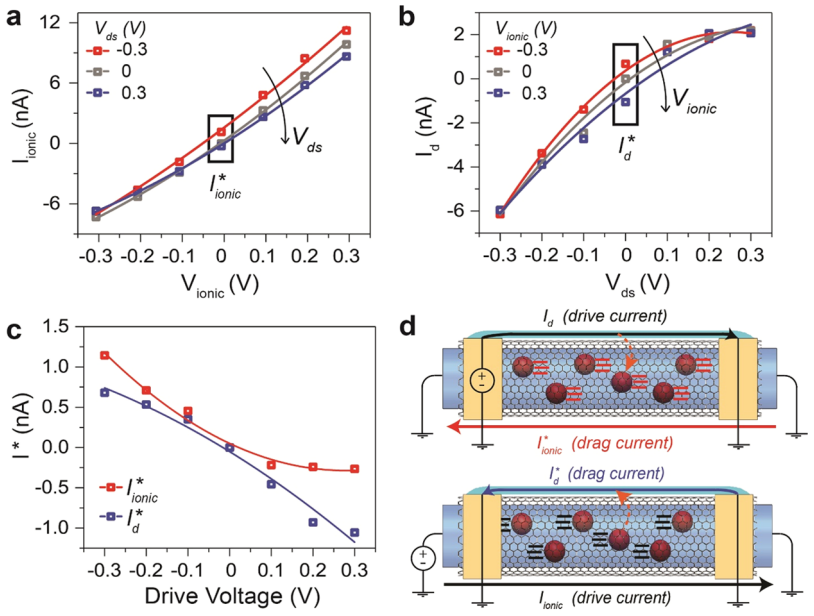

Figure 2. Mutual Coulomb drag energy transfer in Device A with 10 mM electrolyte. (a) Modulation of I_{ionic} by sweeping V_{ds}. (b) Modulation of I_d by sweeping V_{ionic}. (a, b) Coulomb drag results in short-circuit currents (I^*_{ionic}, I^*_d) being recorded with V_{ionic} (V_{ds}) = 0 V (boxed regions). The potential difference applied across the alternate conduction layer is the drive layer voltage. (c) I^*_{ionic} (red) and I^*_d (blue) as functions of drive voltages. (d) Schematic illustration of Coulomb drag interactions. With a voltage applied across the drive layer and the drag layer short-circuited, mobile charge in the drive layer induces transport in quiescent charge in the drag layer. Coulomb drag is repulsive due to currents being primarily comprised of positive charges (cations, holes).

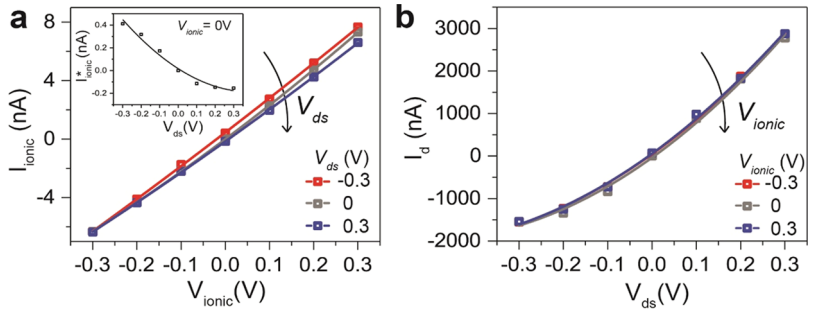

Figure 3. One-directional Coulomb drag energy transfer in device B with 10 mM electrolyte. (a) Modulation of I_{ionic} by sweeping V_{ds}. (inset) I^*_{ionic} versus V_{ds}. (b) When $I_d \gg I_{ionic}$, I_d is minimally modulated with V_{ionic} and I^*_d is below the noise floor.

recorded as averages with minimum integration times of 2 s, yielding signal-to-noise ratios above 9. The subsequent discussion focuses on three representative devices; characterizations of all working devices in 10 mM electrolyte are provided in Table S1. Ionic leakage paths through a polymer layer eventually develop in many of these devices and are evidenced by abrupt orders-of-magnitude increases in ionic current magnitudes. All reported measurements are recorded before these leakage currents appear.

Figure 2 shows I_{ionic} versus V_{ionic} when varying V_{ds} (Figure 2a) and I_d versus V_{ds} when varying V_{ionic} (Figure 2b) for the smallest-diameter SWCNT (Device A) in 10 mM electrolyte. Notably, I_{ionic} is nonzero at V_{ionic} = 0 and I_d is nonzero at V_{ds} = 0 (Figure 2a,b, boxed regions) due to Coulomb drag energy transfer. These short-circuit Coulomb drag currents, denoted I^*_{ionic} and I^*_d, are plotted in Figure 2c versus the corresponding drive layer voltages. Because Coulomb drag currents oppose drive layer voltages, the interlayer interactions are repulsive. The nonlinear dependences of Coulomb drag currents on drive layer voltages are consistent with Figure 2a,b: the larger I^*_d when $V_{ionic} > 0$ results from the larger driving current (I_{ionic}) when $V_{ionic} > 0$ (Figure 2a), while the larger I^*_{ionic} when $V_{ds} < 0$ results from the larger driving current (I_d) when $V_{ds} < 0$ (Figure 2b). In other words, with the electronic circuit as the drive layer, negative I_d exceeds positive I_d (Figure 2b, gray curve), such that I^*_{ionic} is largest for negative drive voltages (Figure 2c, red curve). With the ionic circuit as the drive layer, positive I_{ionic} exceeds negative I_{ionic} (Figure 2a, gray curve), such that I^*_d is largest for positive drive voltages (Figure 2c, blue curve).

This observation that larger drive currents induce larger drag currents is consistent with the proposed Coulomb drag energy transfer mechanism. The top (bottom) of Figure 2d qualitatively depicts these repulsive Coulomb interactions driving I^*_{ionic} and I^*_d. Upon short-circuiting the ionic (electronic) circuit and applying a potential difference across the electronic (ionic) circuit, energy transfers from the mobile electronic (ionic) charge to the quiescent ionic (electronic) charge, dragging a current through the short-circuited layer. Drive and drag layer currents oppose each other due to cations being the primary current carrier in the SWCNT core and

DOI: 10.1021/acs.nanolett.9b04552
Nano Lett. XXXX, XXX, XXX−XXX

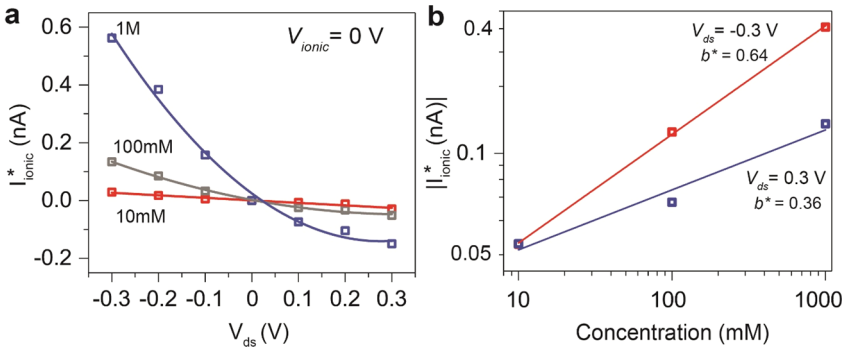

Figure 4. Concentration-dependent scaling of Coulomb drag currents in Device C. (a) I^*_{ionic} versus V_{ds} at varying electrolyte concentrations. I^*_{ionic} scales through concentrations where Debye screening lengths are shorter than the SWCNT radius (0.75 nm). (b) $|I^*_{ionic}|$ versus concentration, with $V_{ds} = \pm 0.3$ V. I^*_{ionic} scales faster when $V_{ds} = -0.3$ V ($b^* = 0.64$) than when $V_{ds} = 0.3$ V ($b^* = 0.36$) due to the field-effect where negative (positive) V_{ds} draws more (fewer) cations into the SWCNT core. I^*_{ionic} scales faster with concentration than ionic conductance ($b = 0.25$, Table S1).

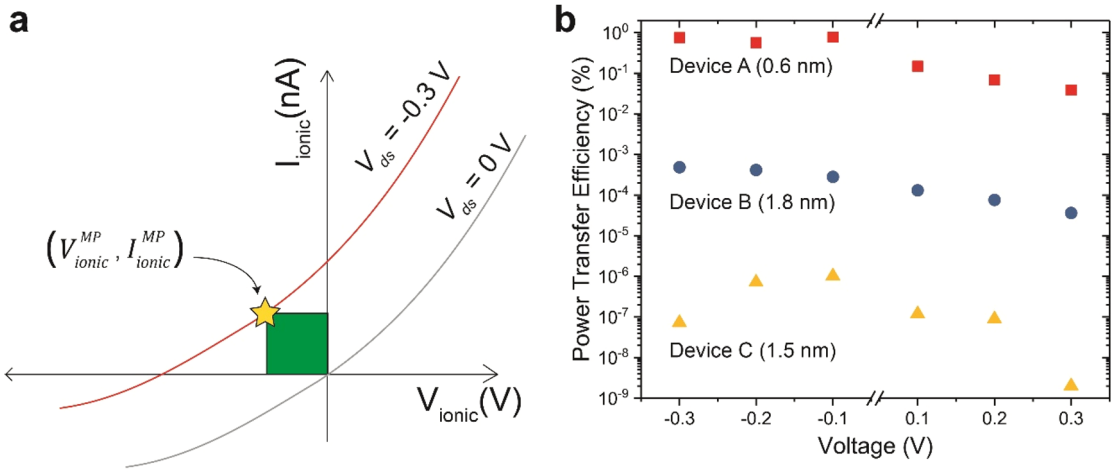

Figure 5. Efficiency of active Coulomb drag ion transport. (a) Schematic depiction of the active transport region, where I_{ionic} opposes V_{ionic} due to Coulomb drag current. Transport energy is transduced from the electronic regime to the ionic regime. The operating conditions for maximum transport efficiency (V^{MP}_{ionic}, I^{MP}_{ionic}) are given by the maximum power rectangle. (b) Maximum transport efficiency (η) for Devices A–C, defined as $\eta = \frac{V^{MP}_{ionic} I^{MP}_{ionic}}{V_{ds} I_d}$.

holes being the primary current carrier along the SWCNT shell.

Device A shows mutual Coulomb drag because I_d and I_{ionic} are of comparable magnitude. It is more typical that $I_d \gg I_{ionic}$ due to the high electrical conductivity of SWCNTs, as illustrated by Device B in 10 mM electrolyte. For this device, Figure 3 shows I_{ionic} versus V_{ionic} when varying V_{ds} (Figure 3a) and I_d versus V_{ds} when varying V_{ionic} (Figure 3b). Under these $I_d \gg I_{ionic}$ conditions, I_d drives I^*_{ionic} (Figure 3a, inset) but I_{ionic} is too small to drive I^*_d above the noise floor. Thus, the I_{ionic}–V_{ionic} characteristics of Devices A and B show a similar V_{ds} dependence, while the I_d–V_{ds} characteristics of Device B show a minimal dependence on V_{ionic}.

We identify the influences of SWCNT diameter and field-effect gating on Coulomb-drag-induced ion pumping by comparing I^*_{ionic} signals between Devices A and B. Because the reductions in I^*_{ionic} between Figure 2c and Figure 3a (inset) are similar to the diameter ratio between the SWCNTs (0.6 and 1.8 nm, respectively; Table S1), we propose that Coulomb drag coupling is enhanced in smaller-diameter SWCNTs. However, the correlation between I_d and I^*_{ionic} magnitudes in Device A is not reproduced in Device B, where positive I_d exceeds negative I_d (Figure 3b), yet negative I^*_{ionic} exceeds positive I^*_{ionic} (Figure 3a, inset). We attribute this discrepancy to field-effect gating of I_{ionic} by V_{ds}, in which the V_{ds} field modulates the cation concentration within the SWCNT.[5] In this model, a negative V_{ds} signal increases the cation concentration within the SWCNT core, while a positive V_{ds} signal reduces it, complicating the relationship between drive and drag layer currents.

We study the concentration dependence of Coulomb drag ion pumping with Device C (10 mM characterization in Figure S7), which is similar in diameter to Device B and measured through 1 M electrolyte conditions. Figure 4a depicts I^*_{ionic} versus V_{ds} in 10 mM, 100 mM, and 1 M electrolytes. Coulomb drag scales beyond conditions where Debye screening lengths are comparable to or less than the SWCNT radius (0.75 nm, Table S1), as evidenced by I^*_{ionic} increasing with concentration across all drive voltages. The field-effect gating of the SWCNT core with V_{ds} is preserved, as positive I^*_{ionic} magnitudes exceed negative magnitudes under all conditions, consistent with the trends in Figures 2c and 3a. Recalling the relationship $G_{ionic} \approx c^b$, we compare Coulomb drag current scaling to ionic conductivity scaling. Figure 4b plots I^*_{ionic} magnitudes versus electrolyte concentrations for $V_{ds} = \pm 0.3$ V, with the slopes of linear fits to the log–log data denoted b^*. The scaling factor for positive I^*_{ionic} is ~250% greater than that for G_{ionic} (Figure 4b, red curve, $b^* = 0.64$ versus $b = 0.25$), while the scaling

DOI: 10.1021/acs.nanolett.9b04552
Nano Lett. XXXX, XXX, XXX–XXX

factor for negative I^*_{ionic} is ~50% greater (Figure 4b, blue curve, $b^* = 0.36$). The dependence of I^*_{ionic} scaling on the sign of V_{ds} is also attributed to the V_{ds}-induced field-effect gating of electrolyte concentration.

To establish our SWCNT device as a biomimetic ion pump, it must actively transport ions against electrolyte potential differences. Active transport is achieved when Coulomb drag is substantial enough that I_{ionic} opposes V_{ionic}. The energy transduction under these conditions is equal to the product of I_{ionic} and V_{ionic}, and operating conditions for maximum efficiency (I^{MP}_{ionic}, V^{MP}_{ionic}) are determined by a maximum power rectangle (Figure 5a). In Figure 5b, we determine the maximum power transfer efficiencies for Devices A–C at 10 mM as a function of V_{ds}, defining efficiency as $\eta = \frac{V^{MP}_{ionic} I^{MP}_{ionic}}{V_{ds} I_d}$. The narrowest SWCNT (Device A) shows three orders of magnitude better efficiency than the wider Device B, suggesting that single-file transport is most conducive to Coulomb drag.[9,17] The efficiency differences between similarly sized Devices B and C suggest that η is strongly affected by parameters other than the SWCNT diameter, including Schottky barrier heights, chemical functionalization of SWCNT ends, and SWCNT impurities or defects. We predict that efficiency would be improved by increasing the spacing between the source and drain electrodes, which would provide a greater surface area for Coulomb interactions.

In conclusion, we demonstrate mutual Coulomb drag coupling between ionic and electronic charge within a single SWCNT. Electronic currents along the SWCNT shell drag ions through the SWCNT core, yielding an electrically actuated biomimetic ion pump that can transport electrolyte without requiring an electrolyte potential difference or pressure gradient. The solid-state electronic input controls the direction and magnitude of ion pumping, with Coulomb drag coupling scaling through 1 M electrolyte concentrations. Transport through the SWCNT core resembles biological ion channel transport, rejecting macromolecules and capable of selectively transporting cations or anions, based on chemical functionalization. As a controllable and selective ion pump, the SWCNT device is a promising tool for biomimetic ion transport in biosensing, nanofluidic, and filtration applications.

Methods. *CNT Growth and Device Fabrication.* Carbon nanotubes were grown with iron-stored ferritin catalysts (Sigma-Aldrich, from equine spleen CAS number 9007-73-2) and chemical vapor deposition, on 2 cm × 2 cm, highly doped 0.001–0.005 Ω-cm Si chips coated with 285 nm of SiO_2. After an air anneal, the system was flushed with argon and hydrogen gas to reduce and activate the catalyst. The furnace temperature was then raised to 890 °C, after which controlled rates of argon and hydrogen gas flowed over and vaporized ice cold ethanol to provide a carbon source for the nanotube growth process, which lasted 1 h. SWCNT growth was imaged in a scanning electron microscope until a suitable nanotube was found, that is, one that was single-walled, sufficiently long, and not overlapping other nanotubes.

After finding an appropriate SWCNT, atomic force microscopy was used to determine its diameter. Source–drain electrodes with 4 μm width and 10 μm spacing were patterned using electron beam lithography (Nanobeam NB4 tool). 100 nm gold electrodes were deposited using electron beam evaporation (Angstrom Evovac deposition system) with adhesive layers of chrome (2 nm) and palladium (10 nm). A subsequent layer of PMMA (Microchem) was spun and patterned as a resist mask, to remove all other nanotubes with oxygen plasma (15 s duration).

Finally, two reservoirs were patterned in another layer of PMMA resist. The extremities of the SWCNT were exposed to oxygen plasma (5 s duration) to truncate and functionalize the ends at known locations. Approximately one in three plasma treatments successfully opened SWCNTs without creating a leakage path. A pre-prepared system of fluid ducts embedded in polydimethylsiloxane (PDMS) (Sylgard 184) was stamped over the chip, such that the channels were aligned over the PMMA reservoirs and the source–drain electrode contacts remained exposed. Ag/AgCl electrodes (BASi systems) were used to access the KCl reservoirs (Fisher Scientific, NH, USA, part number: 7447-40-7) via tubing through the PDMS, and the entire chip was placed in a 3D printed mold. The mold interfaced pins with the electrodes inside the CNT device, breaking out the electronic and ionic signals to benchtop electronics.

Data Acquisition and Analysis. Two low noise current preamplifiers (Stanford Applied Research, SR570) were employed to apply V_{ds} and V_{ionic} to electrodes and measure the resulting currents. Offsets were compensated to ensure I_d and I_{ionic} were zero at $V_{ds} = V_{ionic} = 0$ V. Preamplified current values were acquired using a DAQ card (National Instruments) sampled at 20 kHz. Data was subsequently analyzed using MATLAB.

■ ASSOCIATED CONTENT

Supporting Information

The Supporting Information is available free of charge at https://pubs.acs.org/doi/10.1021/acs.nanolett.9b04552.

Device overview, AFM inspection of SWCNTs, electronic SWCNT conductance, ionic SWCNT conductance, characteristics of all working devices, interlayer coupling, and device C characterization (PDF)

■ AUTHOR INFORMATION

Corresponding Author

*E-mail: shepard@ee.columbia.edu.

ORCID

Jake Rabinowitz: 0000-0001-9671-6860

Author Contributions

C.C. performed the experiments, and J.R., C.C., and K.L.S. analyzed the data and wrote the manuscript.

Notes

The authors declare no competing financial interest.

■ ACKNOWLEDGMENTS

This work was supported in part by the National Institutes of Health under grants R01HG009189 and R01HG006882. The authors would like to acknowledge use of the Columbia Nano Initiative facilities for device fabrication and characterization.

■ REFERENCES

(1) Tans, S. J.; Verschueren, A. R. M.; Dekker, C. Room-Temperature Transistor Based on a Single Carbon Nanotube. *Nature* **1998**, *393*, 49–52.

(2) Rosenblatt, S.; Yaish, Y.; Park, J.; Gore, J.; Sazonova, V.; McEuen, P. L. High Performance Electrolyte Gated Carbon Nanotube Transistors. *Nano Lett.* **2002**, *2*, 869–872.

(3) White, C. T.; Todorov, T. N. Carbon Nanotubes as Long Ballistic Conductors. *Nature* **1998**, *393*, 240–241.

DOI: 10.1021/acs.nanolett.9b04552
Nano Lett. XXXX, XXX, XXX–XXX

(4) Javey, A.; Guo, J.; Wang, Q.; Lundstrom, M.; Dai, H. Ballistic Carbon Nanotube Field-Effect Transistors. *Nature* **2003**, *424*, 654−657.
(5) Pang, P.; He, J.; Park, J. H.; Krstić, P. S.; Lindsay, S. Origin of Giant Ionic Currents in Carbon Nanotube Channels. *ACS Nano* **2011**, *5*, 7277−7283.
(6) Secchi, E.; Nigues, A.; Jubin, L.; Siria, A.; Bocquet, L. Scaling Behavior for Ionic Transport and Its Fluctuations in Individual Carbon Nanotubes. *Phys. Rev. Lett.* **2016**, *116*, 154501.
(7) Amiri, H.; Shepard, K. L.; Nuckolls, C.; Hernández Sánchez, R. Single-Walled Carbon Nanotubes: Mimics of Biological Ion Channels. *Nano Lett.* **2017**, *17*, 1204−1211.
(8) Majumder, M.; Chopra, N.; Andrews, R.; Hinds, B. J. Nanoscale Hydrodynamics: Enhanced Flow in Carbon Nanotubes. *Nature* **2005**, *438*, 44.
(9) Tunuguntla, R. H.; Henley, R. Y.; Yao, Y. C.; Pham, T. A.; Wanunu, M.; Noy, A. Enhanced Water Permeability and Tunable Ion Selectivity in Subnanometer Carbon Nanotube Porins. *Science* **2017**, *357*, 792−796.
(10) McEuen, P. L.; Fuhrer, M. S.; Park, H. Single-Walled Carbon Nanotube Electronics. *IEEE Trans. Nanotechnol.* **2002**, *1*, 78−85.
(11) Heinze, S.; Tersoff, J.; Martel, R.; Derycke, V.; Appenzeller, J.; Avouris, P. Carbon Nanotubes as Schottky Barrier Transistors. *Phys. Rev. Lett.* **2002**, *89*, 106801.
(12) Hou, X.; Guo, W.; Jiang, L. Biomimetic Smart Nanopores and Nanochannels. *Chem. Soc. Rev.* **2011**, *40*, 2385−2401.
(13) Shen, Y.; Saboe, P. O.; Sines, I. T.; Erbakan, M.; Kumar, M. Biomimetic Membranes: A Review. *J. Membr. Sci.* **2014**, *454*, 359−381.
(14) Wu, J.; Gerstandt, K.; Zhang, H.; Liu, J.; Hinds, B. J. Electrophoretically Induced Aqueous Flow through Single-Walled Carbon Nanotube Membranes. *Nat. Nanotechnol.* **2012**, *7*, 133−139.
(15) Corry, B. Water and Ion Transport through Functionalised Carbon Nanotubes: Implications for Desalination Technology. *Energy Environ. Sci.* **2011**, *4*, 751−759.
(16) Choi, W.; Ulissi, Z. W.; Shimizu, S. F. E.; Bellisario, D. O.; Ellison, M. D.; Strano, M. S. Diameter-Dependent Ion Transport through the Interior of Isolated Single-Walled Carbon Nanotubes. *Nat. Commun.* **2013**, *4*, 2397.
(17) Zuo, G.; Shen, R.; Ma, S.; Guo, W. Transport Properties of Single-File Water Molecules inside a Carbon Nanotube Biomimicking Water Channel. *ACS Nano* **2010**, *4*, 205−210.
(18) Narozhny, B. N.; Levchenko, A. Coulomb Drag. *Rev. Mod. Phys.* **2016**, *88*, 025003.
(19) Kim, S.; Jo, I.; Nah, J.; Yao, Z.; Banerjee, S. K.; Tutuc, E. Coulomb Drag of Massless Fermions in Graphene. *Phys. Rev. B: Condens. Matter Mater. Phys.* **2011**, *83*, 161401.
(20) Schütt, M.; Ostrovsky, P. M.; Titov, M.; Gornyi, I. V.; Narozhny, B. N.; Mirlin, A. D. Coulomb Drag in Graphene near the Dirac Point. *Phys. Rev. Lett.* **2013**, *110*, 026601.
(21) Li, J. I. A.; Taniguchi, T.; Watanabe, K.; Hone, J.; Levchenko, A.; Dean, C. R. Negative Coulomb Drag in Double Bilayer Graphene. *Phys. Rev. Lett.* **2016**, *117*, 046802.
(22) Král, P.; Wang, B. Material Drag Phenomena in Nanotubes. *Chem. Rev.* **2013**, *113*, 3372−3390.
(23) Lee, K.; Xue, J.; Dillen, D. C.; Watanabe, K.; Taniguchi, T.; Tutuc, E. Giant Frictional Drag in Double Bilayer Graphene Heterostructures. *Phys. Rev. Lett.* **2016**, *117*, 046803.
(24) Král, P.; Shapiro, M. Nanotube Electron Drag in Flowing Liquids. *Phys. Rev. Lett.* **2001**, *86*, 131−134.
(25) Yuan, Q.; Zhao, Y. P. Hydroelectric Voltage Generation Based on Water-Filled Single-Walled Carbon Nanotubes. *J. Am. Chem. Soc.* **2009**, *131*, 6374−6375.
(26) Ghosh, S.; Sood, A. K.; Kumar, N. Carbon Nanotube Flow Sensors. *Science* **2003**, *299*, 1042−1044.
(27) Zhao, Y.; Song, L.; Deng, K.; Liu, Z.; Zhang, Z.; Yang, Y.; Wang, C.; Yang, H.; Jin, A.; Luo, Q.; et al. Individual Water-Filled Single-Walled Carbon Nanotubes as Hydroelectric Power Converters. *Adv. Mater.* **2008**, *20*, 1772−1776.
(28) Martel, R.; Derycke, V.; Lavoie, C.; Appenzeller, J.; Chan, K. K.; Tersoff, J.; Avouris, P. Ambipolar Electrical Transport in Semiconducting Single-Wall Carbon Nanotubes. *Phys. Rev. Lett.* **2001**, *87*, 256805.
(29) Cui, X.; Freitag, M.; Martel, R.; Brus, L.; Avouris, P. Controlling Energy-Level Alignments at Carbon Nanotube/Au Contacts. *Nano Lett.* **2003**, *3*, 783−787.
(30) Scruggs, N. R.; Robertson, J. W. F.; Kasianowicz, J. J.; Migler, K. B. Rectification of the Ionic Current through Carbon Nanotubes by Electrostatic Assembly of Polyelectrolytes. *Nano Lett.* **2009**, *9*, 3853−3859.

DOI: 10.1021/acs.nanolett.9b04552
Nano Lett. XXXX, XXX, XXX−XXX